Groundbreaking Leachate Migration Evaluation through Ground Penetrating Radar in Different Soil Types

Umar, M. S.,[1] Ghazali, M. D.,[1*] Saputra, H.,[2] Samad, A. M.,[3] Zainon, O.[4] and Zainuddin, K.[1]
[1]Faculty of Built Environment, Universiti Teknologi MARA, Perlis Branch, Arau Campus, 02600 Arau, Perlis, Malaysia, E-mail: mohdsyuibumar@gmail.com.my, mimidiana@uitm.edu.my,* khairul760@uitm.edu.my
[2]Department of Disaster Management, Postgraduate School, Universitas Airlangga, Indonesia E-mail: hijrah.saputra@pasca.unair.ac.id
[3]Geomatic Science and Natural Resource, Faculty of Built Environment, Universiti Teknologi MARA, Shah Alam, Selangor, Malaysia, E-mail: dr_abdmanansamad@ieee.org
[4]Department of Geoinformation, Faculty of Built Environment and Surveying, Universiti Teknologi Malaysia, 81310 Johor Bahru, Johor, Malaysia, Email: othmanz.kl@utm.my
**Corresponding Author*

DOI: https://doi.org/10.52939/ijg.v21i10.4527

Abstract
Landfill leachate is an exceptionally harmful liquid that originates from the decomposition of organic and biodegradable waste materials that have been transported by water percolating through the soil profile. This study aims to evaluate the accuracy of Ground Penetrating Radar (GPR) electromagnetic signals in identifying landfill leachate across various soil properties as it infiltrates. Continuous 24-hour measurements have been performed on three soil samples (Terap Red, Cherang Hangus, and Sand) contaminated with landfill leachate in controlled conditions using Common-Offset GPR at frequencies of 250 MHz and 800 MHz. The velocity of the GPR signal and the reflection coefficient, R, were computed so as to diagnose the impact of leachate over the GPR radar. Signal-to-noise ratio (SNR) and normalized root means square error (NRMSE are utilized to quantify the accuracy of GPR signal uncertainty with GPR velocity calibrated, v = 0.0729 m. Additionally, 3D-GPR images illustrating time-related, horizontal, and vertical variances in the GPR signal were analyzed. 24 hours subsequent to contamination, sandy soil exhibits a higher reflection value than Terap Red and Cherang Hangus, with R values of 0.053 (250MHz) and 0.050 (800Mhz), respectively. interpretation results are preferable for Terap Red and Cherang Hangus (which contain finer soil particles) in comparison to sandy soil. Conversely, interpretation leachate migration findings are preferable for Terap Red and Cherang Hangus since constituted by finer soil particles as opposed to sandy soil.

Keywords: Ground Penetrating Radar, Leachate, Reflection Coefficient, Wastewater Plums, 3D Interpretation

1. Introduction

Increasing concern over water quality degradation, notably from landfill waste and its health implications, has led to attempts to investigate the adverse effects of landfill waste. Leachates from operational and decommissioned landfills lacking liners may contain hazardous substances, potentially polluting water sources by continuing to migrate through soil [1] and [2]. Identifying the location of landfill discharge prior to its infiltration into water systems is an efficient approach to mitigating groundwater contamination. High-frequency electromagnetic waves (EM) are used in Ground Penetrating Radar (GPR), a non-destructive geophysical method, to examine the subsurface, providing a unique tool for locating the source of landfill leaching.

By identifying untreated landfill leachate channels, GPR is able to provide significant information pertaining to the leachate concentration in the soil [3][4] and [5]. This technology is increasingly seen as a viable alternative to traditional groundwater monitoring, especially in landfill sites, due to its efficiency and comprehensive evaluation of water quality.

Despite its potential, the current approach of detecting leachate using GPR are unable to effectively assess the accuracy of their results and impeded by limitations, such as the interference of varying soil dielectric properties with GPR signals [6] and [7]. The variation in dielectric properties is reliant upon the type of soil and specific environmental factors, such as the degree of compactness and moisture level [8]. Particularly in soils such as sand, which reflect GPR signals more intensely than clay, these variations may render it challenging to differentiate between leachate and other subsurface features [9] and [10]. Furthermore, conventional approaches frequently rely on static monitoring of groundwater, which often fails to detect leachate plumes until it has already infiltrated the water table. This limitation restricts the timely identification and remediation of hazardous pollutants.

The proposed method aims to address these deficiencies by incorporating GPR with continuous soil moisture content monitoring, thereby enhancing the sensitivity and accuracy of leachate detection. By correlating real-time soil moisture data with GPR results, this approach not only enhances detection capabilities in diverse soil types but also enhances understanding of leachate distribution and penetration of leachate dynamics. Furthermore, the integration of advanced 3D scanning techniques, such as B-Scan and C-Scan, provides detailed subsurface imaging [11] and [12]. These 3D scanning methods significantly enhance the accuracy and efficiency of leachate detection [13] thereby providing valuable insights for decision-making processes related to environmental remediation and protection [9][14] and [15]. GPR provides 3D data images that allow for a thorough visualization of subsurface structures or anomalies. Researchers use this technique to accurately monitor the movement of untreated waste leachate, gaining detailed information about soil distribution [16]. This highlights the importance of high-quality 3D imaging for accurate identification and visualization of leachate plumes. This significantly helps in determining the extent of the pollution's underground distribution, thereby simplifying the process of devising a more effective remediation strategy. This clarity facilitates the development of remediation strategies that are more effective.

2. Study Area and Datasets

2.1 Study Area

The study area is at the UiTM located in Arau, Perlis, and allocated at coordinate (6.4521° N, 100.2778° E) as shown in Figure 1. A set of tests were carried out on a model tank made of concrete blocks measuring 3.0 x 2.5 x 2.0 meters and having a 5 cm thickness, as seen in (Figure 2). The leachate simulation site and the surrounding area are separated by a barrier marked with highly conductivity concrete blocks. Concrete blocks would have a clearly different dielectric effect on GPR reflections and aid in the control of EM wave propagation on GPR. As depicted in Figure 3, a 15º inclined PVC pipe was installed to enable the subsurface water runoff of wastewater. Three types of soil with different properties, namely Terap Red, Cherang Hangus, and Sandy soil, were located in a simulated tank with dividers manufactured of resistant wood.

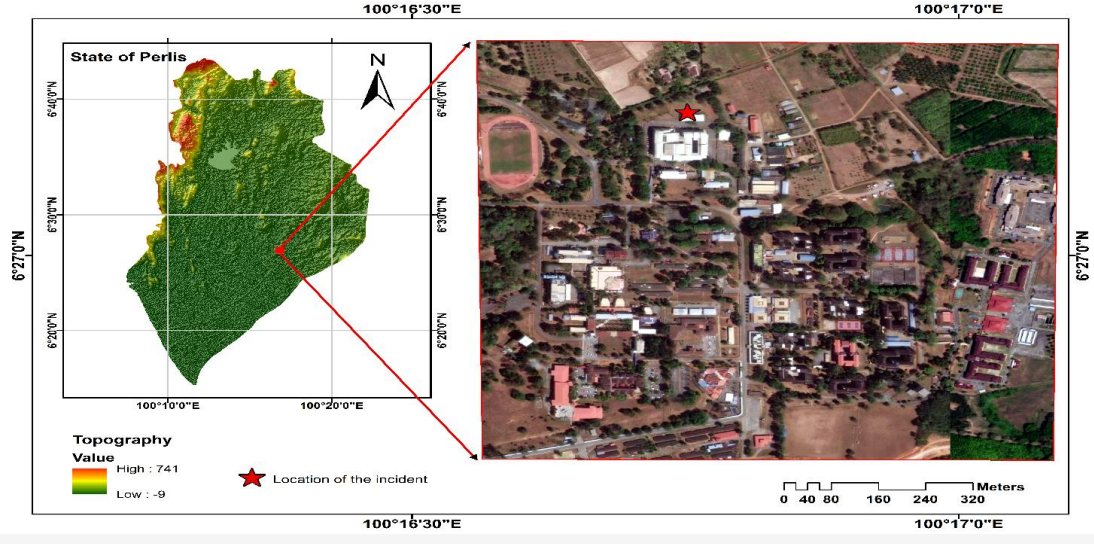

Figure 1: The location map of UiTM at Arau, Perlis

Figure 2: A simulation leachate tank of 3.0 x 2.5 x 2.0 meters and 5 cm in thickness

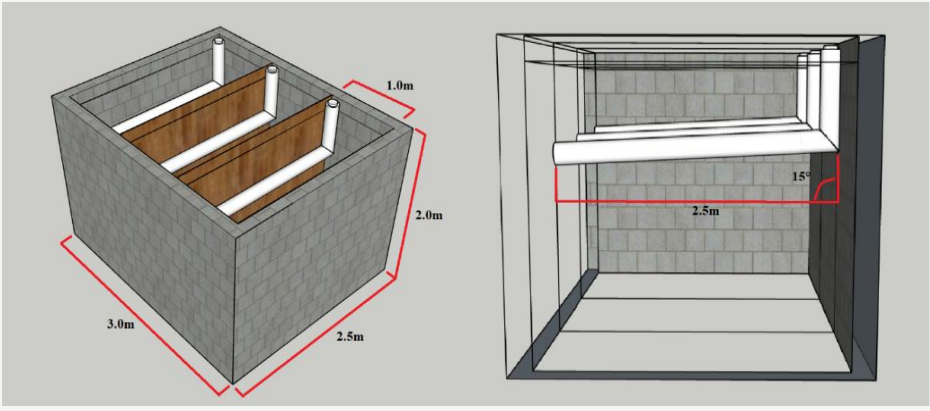

Figure 3: Pipe design for wastewater drains in simulation leachate tank

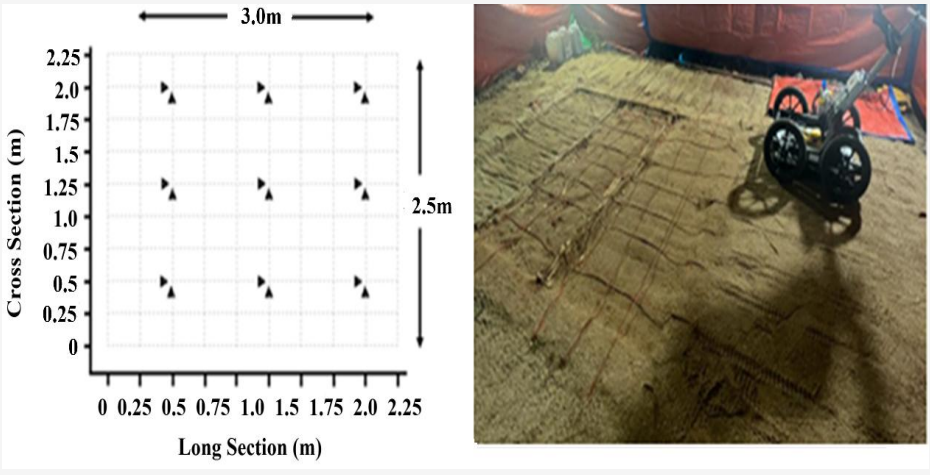

Figure 4: Gridline with 0.25 m spacing between each grid and direction of scanning

3. Method

3.1 Data Collection and Processing

GPR measurements using 250MHz and 800MHz for subsurface wastewater detection were performed between 8 a.m. and 8 p.m. at temperatures of 28.9 and 28.4 ℃, with soil moisture levels of 24.4% and 33.9%, respectively. GPR common-offset frequencies of 250MHz and 800MHz were employed to obtain a B-Scan radargram image on a 0.25m grid using measurements, just as shown in Figure 4. The detection of wastewater is carried out in accordance with the measurement and post-processing parameter settings stated in Table 1 to ensure that the obtained B-Scan data are of high quality and easily interpretable.

Table 1: GPR apparatus and GPR processing parameter for 250MHz in ReflexW software

Parameter Setting	**Frequency**	
Measurement Setting	**250 [MHz]**	**800 [MHz]**
Antenna Separation	0.31m	0.14m
Sample	512	512
Time Window	170.342ns	52.9301ns
Sampling Frequency	3005.72MHz	9673.13MHz
Post-Processing		
Time Zero	-8.75793	-2.93615
Dynamic Correction	0.31m	0.14m
Dewow Filtering	170.342ns	52.9301ns
Bandpass Filtering	125-375	400-1200
Gain Function	5 db/m	5 db/m
Hyperbola Fitting	0.0729	0.0729

Soil moisture content was also measured during GPR measurements to assess the effect of soil moisture from wastewater on the GPR reflection signal.

3.2 Image Identification and Accuracy Analysis

The GPR signal actively identifies the wastewater plume in the subsurface based on the total amplitude of the reflection wave that results from the contrast between dielectrics. The reflection coefficient (*R)* illustrates how the amplitude of the reflected wave is determined as the ratio of the dielectric constants of the two materials. The coefficient *R* is defined in Equation1.

$$R = \frac{\sqrt{\varepsilon_2} - \sqrt{\varepsilon_1}}{\sqrt{\varepsilon_2} + \sqrt{\varepsilon_1}}$$

Equation 1

Where ε_1 and ε_2 represent, respectively, the upper and lower layers of the medium's dielectric constants. By comparing the electromagnetic wave velocity (v) in the medium to the EM wave velocity in vacuum, or the speed of light in free space (c = 0.3 m/ns), one may determine the dielectric characteristics [17] defined as in Equation 2. By considering three types of soil as low-loss non-magnetic materials: Cherang Hangus, Terap Red, and Sandy, relative magnetic permeability, μ= 1 [17].

$$v = \frac{c}{\sqrt{\varepsilon_r \mu_2}}$$

Equation 2

The GPR signal can be more accurately interpreted by assessing the accuracy of the data with assessments such as signal-to-noise ratio (SNR) and normalized root mean square error (NRMSE). SNR is the ratio of the desired information or signal power to the undesired signal or background noise power as presented in Equation 3.

$$SNR = 10\log_{10} \frac{\sum_K^N r(k)^2}{\sum_K^N [f(k) - r(k)]^2}$$

Equation 3

The variable *r(k)* stands for the de-noised or processed signal at index *k*, while *f(k)* represents the original or raw GPR signal containing noise at the same index *k*. With these values, Equation 3 is used to calculate the ratio of the power of the received signal to the power of the noise. SNR provides a quantitative measure of signal quality in the presence of noise, helping to assess how strong the signal is relative to the interfering background noise. While NRSME represented the amplitude or signal of the original data between corresponding de-noised or processed amplitude which is defined in Equation 4 [18],

$$NRMSE = \sqrt{\frac{[f(k) - r(k)]^2}{[f(k) - \mu(k)]^2}}$$

Equation 4

Where *f(k)* represents the original signal at index *k*, *r(k)* represents the de-noised signal at index *k*, and $\mu(k)$ represents the mean value of the original signal across all indices *k*. The NRSME clarifies the proximity of the de-noised amplitude of the GPR signal to that of the original signal.

4. Result and Analysis

4.1 Leachate Evaluation Using 250- and 800-MHz Frequencies

Overall, the GPR survey carried out on laterite soil for wastewater monitoring (Cherang Hangus and Terap Red) and sandy soil revealed that the GPR-800Mhz antenna has a higher resolution for distinguishing targets, as in Figure 5(b), Figure 6(b) and Figure 7(b). The 800MHz-GPR image profiles in Figure 5(b), Figure 6(b), and Figure 7(b) reveal that the high amplitude of the GPR reflection wave of the leachate area is more significant than the GPR-250MHz with their respective reflection coefficients; 0.005 – 0.025 (Cherang Hangus), 0.005 – 0.035 (Terap Red), and 0.015 – 0.050 (Sandy) as displayed in Table 2. Unfortunately, there is a deficiency of high-frequency GPR at 800MHz, which has a short electromagnetic wave and causes a shallow depth of investigation [19] as well as a high rate of attenuation, particularly in areas with high moisture content, like landfill reservoir areas. as [20][21], and [22] concurred. Nevertheless, Figure 5(a), Figure 6(a) and Figure 7(a) illustrated GPR-250MHz radar images with lower resolution, retain the capability to exhibit the contrast of leachate plumes, even in deeper sections surpassing 1 meter.

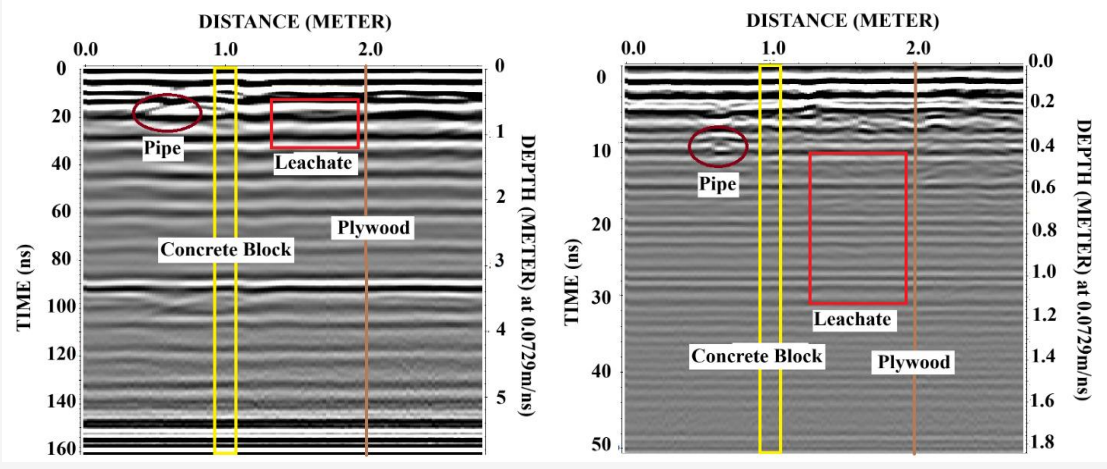

Figure 5: Reflection plume GPR signal to identify leachate migration in Cherang Hangus as well as contains reflection for the pipe to verify the GPR signal, (a) GPR-250MHz and (b) GPR-800MHz

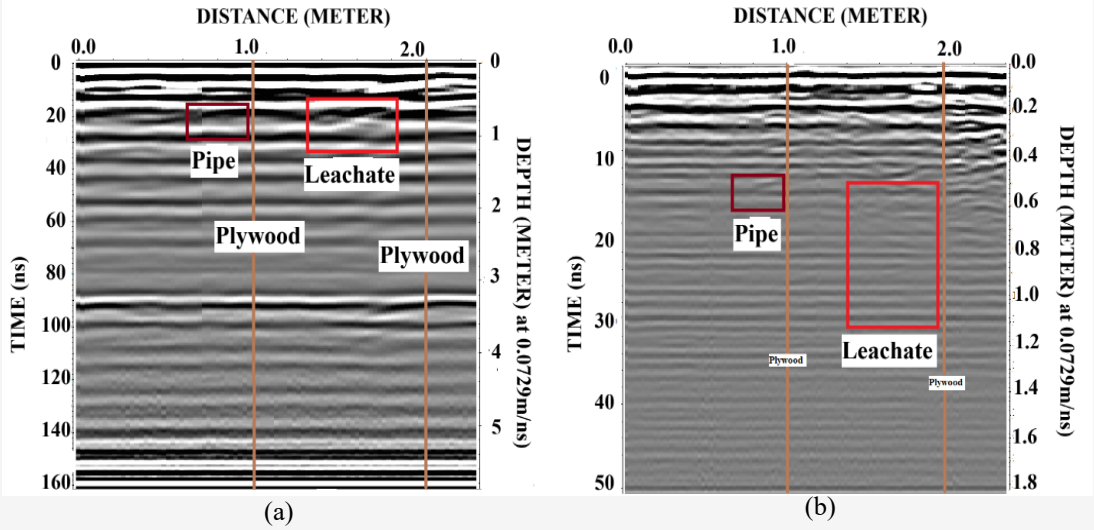

Figure 6. Reflection plume GPR signal to identify leachate migration in Terap Red as well as contain reflection for the pipe to verify the GPR signal, (a) GPR-250MHz and (b) GPR-800MHz

Regrettably, Figure 6(a) presents that the GPR-250MHz capability in sandy soil can produce reflections which are less recognisable, but still have a high reflection coefficient as shown in Table 2. This may be due to the larger grain size of sandy soil compared to Terap Red and Cherang Hangus soils, as determined by the soil sieve tests in Figure 8. In ordinary operation, EM wave velocity is higher and decreases with increasing depth due to an increase in water content and in dry soil conditions with a low dielectric such as sand (2.2881), as shown in Table 3. Yet its opposite condition can occur, particularly in sandy soils with the capacity to retain low water after leachate dispersion events and in soils with ubiquitous sandwich-like structures in which wetter soil layers are disturbed by drier soil layers or vice versa, as mentioned by [23]. Indeed, the functionality of GPR-250MHz to detect the deep depth of laterite soil, which is typically used as landfill soil liner, makes it applicable for landfill implementations, as evidenced by [19] and [22]. The GPR signal image for both GPR frequencies have been calibrated with velocity, v = 0.0729 m/ns; leachate migration can be seen scattered vertically and horizontally with respective depths of 0.6-1.0 (Cherang Hangus), 0.6-0.9 (Terap Red), and 0.6-1.1 (Sandy). It was discovered that the dissolved leachate tends to flow faster in the stratigraphy of Sandy soil compared to Cherang Hangus and Terap Red, in which the leachate migrates slowly to the centre of gravity and is saturated more rapidly (Figure 5(a) and Figure 6(a)).

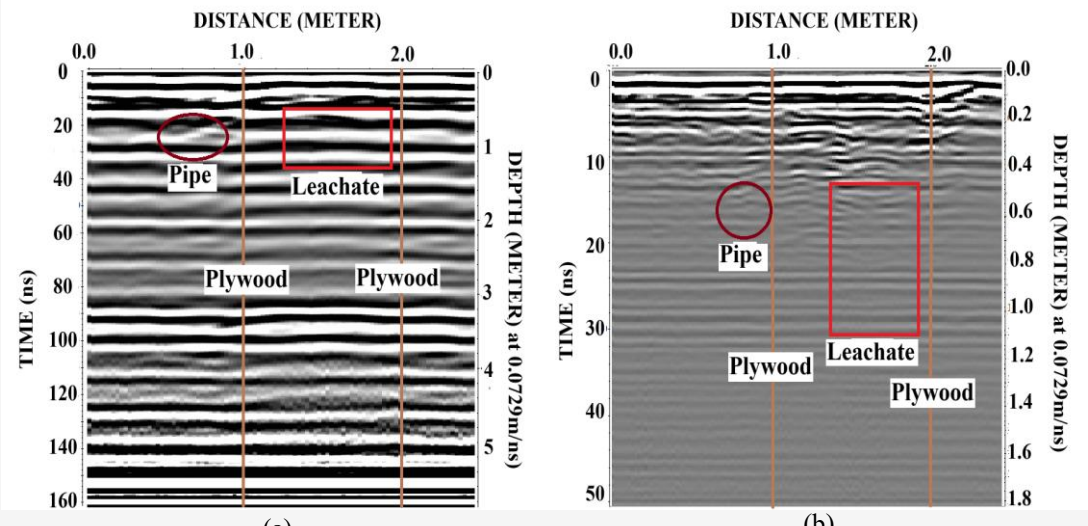

Figure 7: Reflection plume GPR signal to identify leachate migration in Sand as well as containing reflection for the pipe to verify the GPR signal, (a) GPR-250MHz and (b) GPR-800MHz

Table 2: The reflection coefficient (R) of the reflection coefficient (r) of GPR signal for leachate migration identification in three types of soil (Cherang Hangus, Terap Red and Sandy)

Soil	Cherang Hangus				Terap Red				Sand			
Pattern	1		2		1		2		1		2	
	250 MHz											
Times	8am	8pm	8am	8pm	8am	8pm	8am	8pm	8am	8pm	8am	8pm
Velocity 1	0.094	0.094	0.09	0.092	0.114	0.116	0.115	0.111	0.147	0.146	0.129	0.129
Velocity 2	0.093	0.091	0.088	0.089	0.113	0.115	0.111	0.109	0.143	0.143	0.116	0.117
Reflection Coefficient	0.005	0.015	0.010	0.015	0.005	0.005	0.015	0.005	0.015	0.010	0.053	0.050
	800 MHz											
Velocity 1	0.103	0.101	0.110	0.108	0.119	0.123	0.117	0.129	0.146	0.146	0.139	0.139
Velocity 2	0.102	0.099	0.109	0.103	0.118	0.119	0.116	0.120	0.142	0.143	0.125	0.126
Reflection Coefficient	0.005	0.010	0.005	0.025	0.005	0.015	0.005	0.035	0.015	0.010	0.050	0.050
Moisture	17.2	15.8	17.2	15.8	14.1	21.4	14.1	21.4	18.7	19.5	18.7	19.5

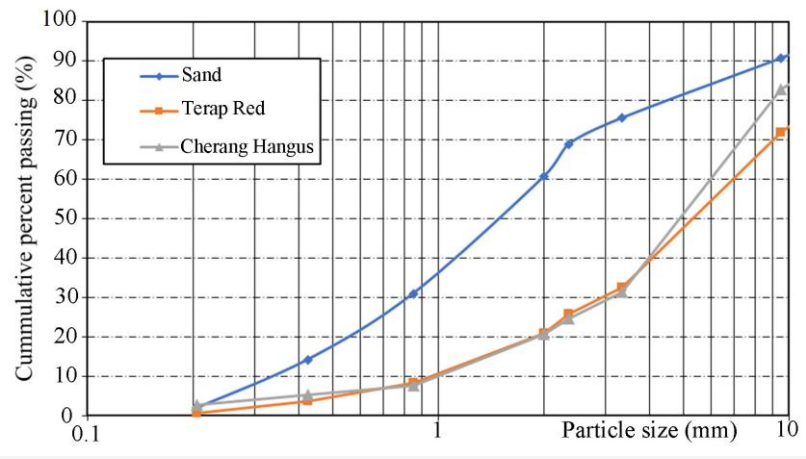

Figure 8: Sieve analysis test for three types of soil (Cherang Hangus, Terap Red and Sandy)

Table 3: Value for the accuracy assessment of the GPR validation component for soil

Type of Accuracy	Type of Soil		
	Cherang Hangus	Terap Red	Sandy Soil
SNR (dB)	24.502	27.307	22.892
NRSME	0.029	0.032	0.033

This migration is likely attributable to the characteristics of sandy soil, which has a high liquid limit, and laterite soil, which has high plastic limit properties as revealed in Table 3 and can retain leachate for long durations. This GPR signal image supports the effectiveness of using laterite soil in landfill areas based on the high adsorption factor of laterite soil. As per [24], laterite soil is beneficial for Freundlich isotherm adsorption of soil, which involves mass transport of the adsorbent from the solution phase to the inner surfaces of the porous adsorbent, where absorption occurs.

Based on the sieve analysis results (Figure 8), all three soils are classified as coarse-grained soils, with less than 5% passing through sieve No. 200. According to the Unified Soil Classification System (USCS), Atterberg limits are not required for these soils, and the classification is determined solely from particle-size distribution. Accordingly, the soil type for Sand is classified as SP (poorly graded sand), while both Terap Red and Cherang Hangus are classified as SW (well-graded sand). Each soil sample has been assigned a single soil type, in line with USCS requirements. Figure 8 illustrates the results of soil sieve tests conducted on the three types of soil used in the study: Terap Red, Cherang Hangus, and sandy soil. The figure presents a comparative analysis of the grain size distribution for each soil type, highlighting the differences in particle size and composition. The data indicates that sandy soil has larger grain sizes compared to Terap Red and Cherang Hangus, which contain finer particles. This distinction is crucial as it impacts the behavior of electromagnetic waves during GPR measurements. The larger grain size in sandy soil can lead to less recognizable reflections in GPR signals, despite having a high reflection coefficient. This information is essential for understanding how different soil types affect GPR's ability to detect leachate migration, thereby influencing the effectiveness of groundwater monitoring strategies.

4.2 GPR-3D Assessment of Leachate Identification

To estimate the migration dispersion of leachate predicated on GPR data, the captured radar tracks were analysed with time-varying attributes. Table 2 revealed that at both frequencies, leachate identification at 8 p.m. exhibited a higher signal reflection coefficient compared favourably to 8 a.m. During the fluctuation in soil moisture caused by changes in daytime and nighttime temperatures, different phases of varying GPR wave velocities will occur, and the drier nature of the material will aid in the wave's travel throughout the soil, as stated by [21]. As performed by [22], in addition to acquire an overall view of leachate migration attributes for geometric and dynamic features, a complex interpretation of 3D GPR data sets sourced from radar wave amplitude analysis of reflected dielectric variations was done. ReflexW uses a linear interpolation method to fill in the gaps between neighbouring GPR lines by importing 2D GPR (as seen in Figures 5, 6, 7) from MALA Groundvision 2.0. (Cross and long section) to create a more understandable solid 3D volume. Figures 9,10 and 11 depict the creation of 2 four different ways 3D-GPR

image maps, also known as a GPR-C-scan, based on two distinct frequencies, time and of leachate migration transition.

The 3D-GPR model sliced in the x, y, and z plane could provide a partial understanding [12] of the leachate migration for the 3D shape, as well as the spatial relationship of the subsurface leachate according to depth (z), as displayed in Figure 9a, 10a and 11a. Trends in leachate migration can be discerned by contrasting amplitude variations from the z plane to GPR-800MHz and GPR-250MHz signal images for two separate GPR detection times. 3D view through x, y, z plane slices entails identifying EM wave signals from low-frequency GPR-250MHz, particularly in sandy soil, which is difficult to interpret with 2D-GPR (see Figure 11(a)). Figure 11(a) reveals that the GPR-250MHz frequency produces a significant change in wave reflection, proving that leachate migration occurs more rapidly and flows vertically in conformance with the saturated soil's more thermally conductive characteristics. Figure 11(a) reveals that the GPR-250MHz frequency produces a significant change in wave reflection, proving that leachate migration occurs more rapidly and flows vertically in conformance with the saturated soil's more thermally conductive characteristics as in Table 3.

On the flip side, Figures 9(a) and Figure 10(a) illustrate insignificant leachate migration at two different times in laterite soil with a low thermal conductivity between 0.6 and 1.3. Soil thermal conductivity is a thermophysical parameter for heat exchange or thermal diffusion properties which is essential for thermal treatment of contaminated soil. 3D-GPR as depicted in Figure 9(b), Figure 10(b), and Figure 11(b) represents the distribution of high-amplitude changes, which allows for a more precise identification of the characteristics of these leachate transitions. This distribution of high amplitude illustrates more clearly the characteristics of soil retention capacity as agreed by [17], which exhibits less variation for laterite soil in Figures 9b and 10b than for sandy soil in Figure 11(b). The properties of the soil have maintained consistent moisture levels and inhibited leachate from quickly penetrating the soil as determined by [25]. This reflection and amplitude distribution can enhance the monitoring system for contaminated soil in a landfill relying on a groundwater monitoring well by evaluating the Water Quality Index outlined by the National Water Quality Standards (NWQS) [26].

The change in soil water content has generated an amplitude variation of the GPR image profile along Line 6, as indicated by the peak amplitude value that is shown. A soil moisture probe was used to track this shift in the moisture content of the soil. The GPR reflection has identified two prominent patterns (P1 and P2) that are believed to depict the migration of natural contamination in the garbage, based on the dielectric change of the soil. It shows that the high water-holding capacity of the soil allows for excellent management of leachate migration via the laterite soil pores. The study [23] on the contamination caused by diesel waste on laterite soil provides evidence for this.

Overall, the analysis of the reflection coefficient highlights the different characteristics of the three soil types. Cherang Hangus soil exhibits consistently low reflection coefficients, indicating efficient leachate migration with minimal energy loss. Terap Red soil shows variation in reflection coefficients based on the pattern, suggesting pattern-dependent energy loss due to reflection. Sandy soil also displays variation in reflection coefficients based on the pattern, with Pattern 2 exhibiting a lower energy loss. Understanding these variations in reflection coefficients can provide valuable insights into the behaviour of leachate migration and the characteristics of different soil types, which can be essential for evaluating leachate management and environmental impact assessments in diverse soil conditions.

4.3 Evaluation of GPR Image Accuracy for Contaminated

The amplitude fluctuation of the raw signal and the GPR procedure (after calibration of the velocity correction) for the reflection profile of line 6 are shown in Figure 12. GPR measurements to track leachate reaction to modifications in simulated tanks. The denoising results of the three methods, signal-to-noise-ratio (SNR), RSMN, and RMSE for GPR signal performance, are quantitatively shown in Table 3 after the images are generated. The results are 24.5021dB for Cherang Hangus, 27.3066dB for Terap Red, and 22.8916dB for sand, which is greater than 15dbB Better denoising performance of GPR data is achieved with higher SNR and lower NRMSE, Higher dB values like Terap Red's 27.3066 dB indicate better fidelity to the original signal after denoising, meaning less residual noise and a clearer output. The reason is that there's more useful information (signal) than unwanted data (noise) in a high SNR output.

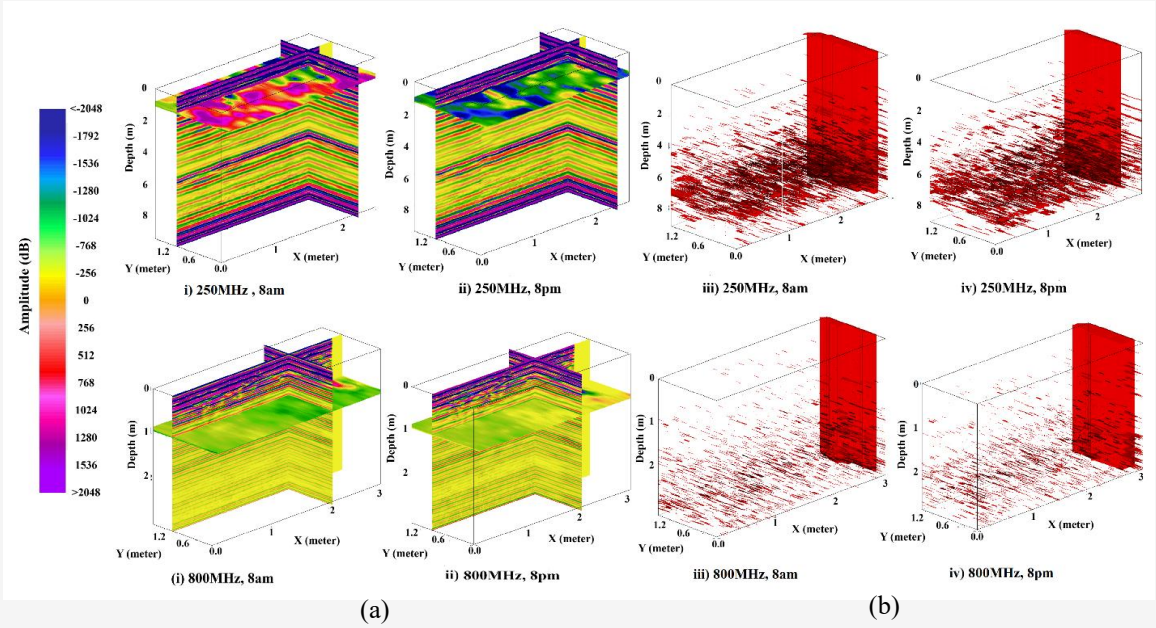

Figure 9: Changes in reflection-processed GPR data for leachate transport in the Cherang Hangus soil in simulation tank:
(a) 3D-GPR cross-section of signal image and (b) Amplitude distribution of leachate areas in 3D-GPR

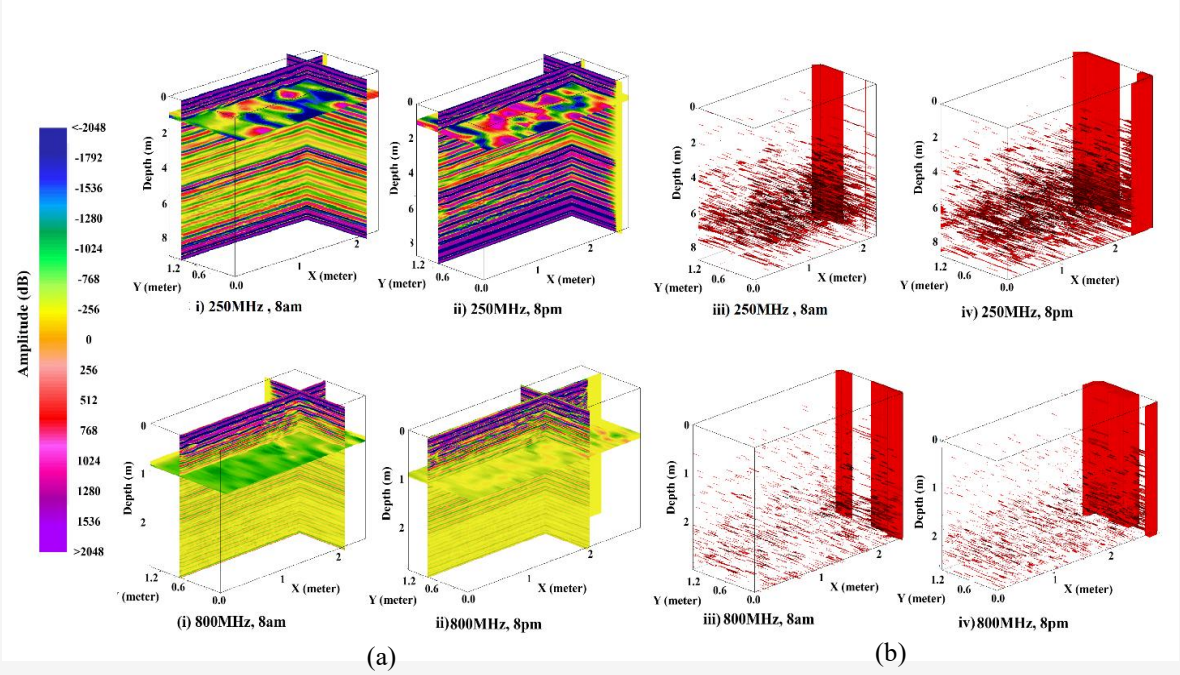

Figure 10: Changes in reflection-processed GPR data for leachate transport in the Terap Red soil in a simulation tank:
(a) 3D-GPR cross-section of signal image and (b) Amplitude distribution of leachate areas in 3D-GPR

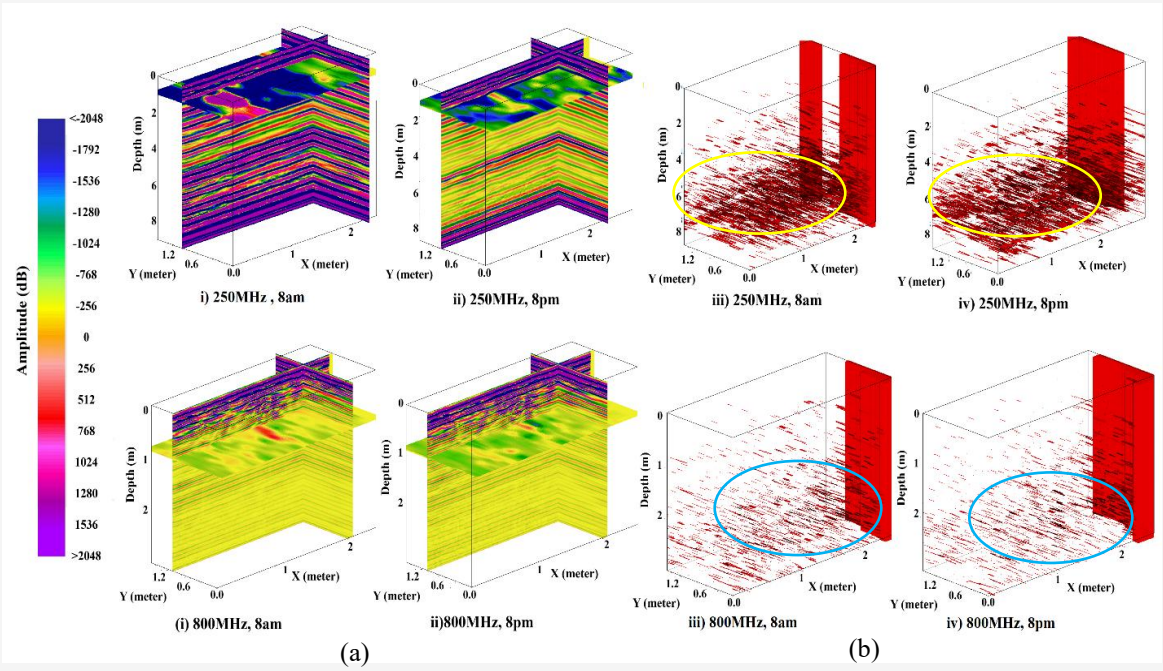

Figure 11: Changes in reflection-processed GPR data for leachate transport in a sandy soil in a simulation tank: (a) 3D-GPR cross-section of signal image and (b) Amplitude distribution of leachate areas in 3D-GPR

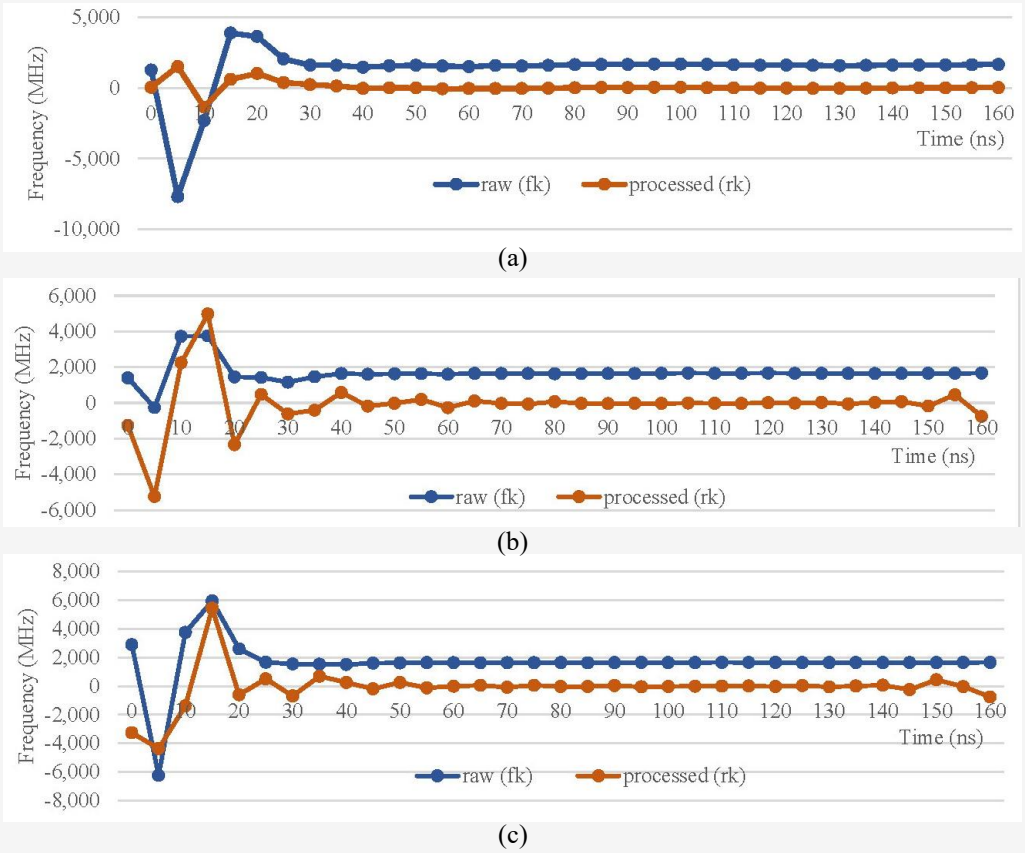

Figure 12: Comparison of the denoised signal and the raw amplitude GPR signal noise for contaminated leachate soil (a) Cherang Hangus (b) Terap Red and (c) Sand

NRMSE complements the SNR metric by focusing on reconstruction accuracy rather than just noise reduction performance. Together, provide a comprehensive evaluation of the denoising process. Acceptable ranges for accuracy evaluation are well established. An SNR above 3 dB is the minimum threshold for reliable subsurface imaging [27] while values greater than 5–10 dB is recommended for clear GPR interpretation. For model validation, an NRMSE ≤ 10% is considered excellent, and values up to 20% remain acceptable for environmental and hydrological studies [28] and [29]. In this study, all soils recorded SNR > 5 dB, confirming strong signal quality. The NRMSE values ranged from 2–12%, with Cherang Hangus and Terap Red falling below 10%, and Sand slightly higher but still within the acceptable 20% limit. Hence, the accuracies obtained in this study are within internationally recognized ranges.

5. Conclusion

The study presented the effectiveness of Ground Penetrating Radar (GPR) in detecting landfill leachate across different soil types, specifically Terap Red, Cherang Hangus, and sandy soil. The research highlights the significant role of GPR as a non-destructive method for monitoring subsurface contamination, particularly in the context of increasing concerns over groundwater quality due to landfill leachate. The results indicate that GPR can successfully identify leachate plumes, with findings showing that sandy soil exhibited higher reflection values compared to the finer soils, Terap Red and Cherang Hangus. However, the interpretation of GPR signals was more favorable in finer soils due to their dielectric properties, which enhance signal clarity. The study underscores the importance of frequency selection in GPR applications, revealing that while higher frequencies (800 MHz) provide better resolution for shallow depths, lower frequencies (250 MHz) are more effective for deeper investigations.

In conclusion, this research contributes valuable insights into the dynamics of leachate migration and emphasizes the need for integrating GPR with continuous soil moisture monitoring to enhance understanding of leachate behavior. The findings advocate for the adoption of GPR technology in environmental assessments and remediation strategies, ultimately aiding in the preservation of water resources and ecosystem integrity. Future studies should explore further variations in soil types and moisture conditions to refine GPR methodologies for broader applications in environmental monitoring.

Acknowledgement

The Ministry of Higher Education Malaysia (MOHE) is to be thanked and acknowledged by the authors for the research grant that was granted. The Fundamental Research Grant Scheme (FRGS) (Reference no: FRGS/1/2021/STG08/UITM/02/1) provided financial support and partial funding for this work named "Geo-Radar Signatures Segmentation for Laterite Soil Wastewater Tomography: Petrophysical Relationship and Cluttering Algorithms Model". The authors would like to thank UiTM for the study site area.

Reference

[1] Naveen, B. P., Mahapatra, D. M., Sitharam, T. G., Sivapullaiah, P. V. and Ramachandra, T. V., (2017). Physico-Chemical and Biological Characterization of Urban Municipal Landfill Leachate. *Environmental Pollution*, Vol. 220, 1–12. https://doi.org/10.1016/j.envpol.2016.09.002.

[2] Ashraf, M. A., Yusoff, I., Yusof, M. and Alias, Y., (2013). Study of Contaminant Transport at an Open-Tipping Waste Disposal Site. *Environmental Science and Pollution Research*, Vol. 20(7), 4689–4710. https://doi.org/10.1007/s11356-012-1423-x.

[3] Liu, X., Chen, J., Cui, X., Liu, Q., Cao, X. and Chen, X., (2019). Measurement of Soil Water Content Using Ground-Penetrating Radar: A Review of Current Methods. *International Journal of Digital Earth*, Vol. 12(1), 95–118. https://doi.org/10.1080/17538947.2017.1412520.

[4] Anbazhagan, P., Bittelli, M., Pallepati, R. R. and Mahajan, P., (2020). Comparison of Soil Water Content Estimation Equations Using Ground Penetrating Radar. *Journal of Hydrology*, Vol. 588, 1-21. https://doi.org/10.1016/j.jhydrol.2020.125039.

[5] Mahmoudzadeh Ardekani, M. R., (2013). Off- and On-Ground GPR Techniques for Field-Scale Soil Moisture Mapping. *Geoderma*, Vol. 200–201, 55–66. https://doi.org/10.1016/j.geoderma.2013.02.010.

[6] Li, Z., Torbaghan, M. E., Zhang, T., Qin, X., Li, W., Li, Y. and Zhang, J., (2024). An Automated 3D Crack Severity Assessment using Surface Data for Improving Flexible Pavement Maintenance Strategies. *IEEE Transactions on Intelligent Transportation Systems*, Vol. 25, 1–14. https://doi.org/10.1109/TITS.2024.3379997.

[7] Li, F., Yang, F., Xie, Y., Qiao, X., Du, C., Li, C., Ru, Q., Zhang, F., Gu, X. and Yong, Z., (2024). Research on 3D Ground Penetrating Radar Deep Underground Cavity Identification Algorithm in Urban Roads Using Multi-Dimensional Time-Frequency Features. *NDT and E International*, Vol. 143, 1-17. https://doi.org/10.1016/j.ndteint.2024.103060.

[8] Kargas, G. and Kerkides, P., (2010). Evaluation of a Dielectric Sensor for Measurement of Soil-Water Electrical Conductivity. *Journal of Irrigation and Drainage Engineering*, Vol. 136(8), 553–558. https://doi.org/10.1061/(asce)ir.1943-4774.0000218.

[9] Iftimie, N., Savin, A., Steigmann, R. and Dobrescu, G., (2021). Underground Pipeline Identification into a Non-Destructive Case Study Based on Ground-Penetrating Radar Imaging. *Remote Sensing*, Vol. 13(17). 1-14. https://doi.org/10.3390/rs13173494.

[10] Badr, M. E., Ali, E. M., Awadalla, K. H. and Sharshar, H. A., (2009). Effects of Soil Physical Properties on Landmines. *Radio Science*, Vol. 44, 1-7. https://doi.org/10.2528/PIERC09012403.

[11] Luo, T. X. H., Lai, W. W. L., Chang, R. K. W. and Goodman, D., (2019). An Empirical Study of GPR Imaging Criteria. *Journal of Applied Geophysics*, Vol. 165, 37–48. https://doi.org/10.1016/j.jappgeo.2019.04.008.

[12] Kelly, T. B., Angel, M. N., O'Connor, D. E., Huff, C. C., Morris, L. E. and Wach, G. D., (2021). A Novel Approach to 3D Modelling Ground-Penetrating Radar (GPR) Data – A Case Study of a Cemetery and Applications for Criminal Investigation. *Forensic Science International*, Vol. 325, 1-15. https://doi.org/10.1016/j.forsciint.2021.110882.

[13] Hou, F., Lei, W., Li, S., Xi, J., Xu, M. and Luo, J., (2021). Improved Mask R-CNN With Distance Guided Intersection over Union for GPR Signature Detection and Segmentation. *Automation in Construction*, Vol. 121, 1-14. https://doi.org/10.1016/j.autcon.2020.103414.

[14] Hassan, A., Razali, M., Sulaiman, S., Idris, A., Ghazali, M., Hashim, M., and Junoh, S. (2023). Accuracy Assessment of GPR Data for Buried Objects with Different Pipes and Soil-Based Conditions. *International Journal of Geoinformatics*, Vol. 19(5), 9–18. https://doi.org/10.52939/ijg.v19i5.2651.

[15] Dell'Acqua, A., Sarti, A., Tubaro, S. and Zanzi, L., (2004). Detection Of Linear Objects in GPR Data. *Signal Processing*, Vol. 84(4), 785–799. https://doi.org/10.1016/j.sigpro.2003.12.010.

[16] Fisika, J., Mipa, F. and Mulawarman, U., (2016). Interpretasi Sedimen Bawah Permukaan Tanah Dengan Menggunakan Metode GPR (Ground Penetrating Radar) Di Daerah Pantai Kulon Progo Daerah Istimewa Yogyakarta [Interpretation of Subsurface Soil Sediments Using GPR Method in the Kulon Progo Coastal Area, Yogyakarta Special Region]. *Pusat Penelitian dan Pengembangan Geologi Kelautan Bandung*, Vol. 1(1). 13-17.

[17] Ghazali, M. D., Zainon, O., Idris, K. M., Zainon, S. N. A., Karim, M. N. A., Anshah, S. A., Talib, N. F. A., (2020). The Assessment of Relative Permittivity on Diesel Vapour in the Moisture Content of Terap Red Soil by Ground Penetrating Radar. *Air, Soil and Water Research*, Vol. 13, 15–17. https://doi.org/10.1177/1178622120930661.

[18] Baili, J., Lahouar, S., Hergli, M., Al-Qadi, I. L. and Besbes, K., (2009). GPR Signal De-Noising by Discrete Wavelet Transform. *NDT and E International*, Vol. 42(8), 696–703. https://doi.org/10.1016/j.ndteint.2009.06.003.

[19] Wijewardana, Y. N. S., Shilpadi, A. T., Mowjood, M. I. M., Kawamoto, K. and Galagedara, L. W., (2017). Ground-Penetrating Radar (GPR) Responses for Sub-Surface Salt Contamination and Solid Waste: Modeling and Controlled Lysimeter Studies. *Environmental Monitoring and Assessment*, Vol. 189(2), https://doi.org/10.1007/s10661-017-5770-4.

[20] Syafalni, S., Dhaarisheni, M., Abustan, I. and Rozainy, M. A. Z. M. R., (2015). Landfill Leachate Treatment by Using Peat Soil and Laterite Soil as Natural Adsorbents. *International Journal of Applied Engineering Research*, Vol. 10(3), 5707–5728. http://www.ripublication.com/ijaer10/ijaerv10n3_27.pdf.

[21] Lai, W. W. L., Chang, R. K. W., Völker, C. and Cheung, B. W. Y., (2021). GPR Wave Dispersion for Material Characterization. *Construction and Building Materials*, Vol. 302. https://doi.org/10.1016/j.conbuildmat.2021.122597.

[22] Halim, N. Z. A., Abdullah, N., Ghazali, M. D. and Hassan, H., (2023). The Possibility of Using Terrestrial-Based Ground Penetrating Radar (GPR) Technology for Supplying 3rd Dimension Information for a Search and Recovery Mission for Landslide Victims. *International Journal of Geoinformatics*, Vol. 19(5), 105–118. https://doi.org/10.52939/ijg.v19i5.2669.

[23] Koyama, C. N., (2017). In-Situ Measurement of Soil Permittivity at Various Depths for the Calibration and Validation of Low-Frequency SAR Soil Moisture Models by Using GPR. *Remote Sensing*, Vol. 9(6), 580. 1-14. https://doi.org/10.3390/rs9060580.

[24] Yochim, A., Zytner, R. G., McBean, E. A. and Endres, A. L., (2013). Estimating Water Content in an Active Landfill with the Aid of GPR. *Waste Management*, Vol. 33(10), 2015–2028. https://doi.org/10.1016/j.wasman.2013.05.020.

[25] Oni, O. A. G. and Ekiti, A., (2016). The Use of Lateritic Soils as a Cover Material in Municipal Solid Waste Landfills in Nigeria. *Journal of Environmental Earth Science*, Vol. 6, 198–205. https://doi.org/10.1061/(ASCE)MT.1943-5533.0000451.

[26] Fadzillah, N., Salim, A. and Kasmin, H., (2022). Study on the Water Quality Index (WQI) of Parit Besar River in Batu Pahat. *Journal of Advanced Environmental Solutions and Resource Recovery*, Vol. 2(1), 8–14. https://doi.org/10.30880/jaesrr.2022.02.01.002.

[27] Annan, A. P., (2009). Electromagnetic Principles of Ground Penetrating Radar. In: Jol, H. (Ed.), *Ground Penetrating Radar: Theory and Applications*. Amsterdam: Elsevier; 1–40. https://doi.org/10.1016/B978-0-444-53348-7.00001-6.

[28] Willmott, C. J. and Matsuura, K., (2005). Advantages of the Mean Absolute Error (MAE) over the Root Mean Square Error (RMSE) In Assessing Average Model Performance. *Climate Research*, Vol. 30(1). 79–82. https://doi.org/10.3354/cr030079.

[29] Moriasi, D. N., Arnold, J. G., Van Liew, M. W., Bingner, R. L., Harmel, R. D. and Veith, T. L., (2007). Model Evaluation Guidelines for Systematic Quantification of Accuracy in Watershed Simulations. *Transactions of the ASABE*, Vol. 50(3), 885–900. https://doi.org/10.13031/2013.23153.